Lucas Harris[1], Linjiong Zhou[2], Alex Kaltenbaugh[1,3], Spencer Clark[1,4], Kai-Yuan Cheng[2], and Chris Bretherton[4,5]

[1]NOAA/Geophysical Fluid Dynamics Laboratory, Princeton, NJ.

[2]Cooperative Institute for Modeling Earth Systems, and Program on Atmospheric and Oceanic Sciences, Princeton University, Princeton, NJ.

[3]University Corporation for Atmospheric Research, Boulder, CO.

[4]Allen Institute for Artificial Intelligence, Seattle, WA.

[5]Department of Atmospheric Sciences, University of Washington, Seattle, WA.

Corresponding author: Lucas Harris (`lucas.harris@noaa.gov`)

Key Points:

- The GFDL X-SHiELD Global Storm-Resolving Model can explicitly represent rotating convection worldwide.
- Cyclonically-rotating updrafts predominate over the oceans and higher latitudes, less so over land and in the deep tropics.
- Environmental controls explain much of the predominance of cyclonic updrafts but internal storm dynamics are also important.

Abstract

We present the characteristics of rotating convective updrafts in the 2021 version of GFDL's Experimental System for High-resolution prediction on Earth-to-Local Domains (X-SHiELD), a kilometer scale global storm resolving model (GSRM). Rotation is quantified using 2–5 km Updraft Helicity (UH) in a year-long integration forced by analyzed SSTs. Updrafts with UH magnitudes above 50 m^2 s^{-2} are common over the mid-latitude continents, especially in the warm seasons where they are associated with severe weather but are also common over most tropical ocean basins. In nearly all areas cyclonically rotating convection dominates, with larger UH values increasingly preferring cyclonic rotation. The ratio of cyclonic to anticyclonic updrafts is largest in the subtropical and mid-latitude oceans and is slightly lower over mid-latitude continents. The ratio of cyclonic to anticyclonic updrafts can be substantively explained by the mean storm-relative helicity (SRH) in convective regions, indicating the importance for environmental controls on the sense of storm rotation, although internal storm dynamics also plays a role in the generation of anticyclonic updrafts.

Plain Language Summary

Thunderstorm updrafts are sometimes observed to rotate. This rotation is important especially in severe thunderstorms and developing hurricanes since it allows an updraft to last longer and become more intense. However, little is known about rotating updrafts outside of these isolated contexts and there is not yet a global survey of this phenomenon. We have developed a new model called X-SHiELD, which is one of an emerging class of atmosphere computer

models that can represent individual thunderstorm updrafts worldwide. This means it can simulate rotating updrafts, unlike traditional global models, and can do so globally unlike regional models for forecasting thunderstorms. We find that rotating thunderstorms are common in many warmer places in the world, even if they are not always as strong as the fearsome severe thunderstorms in the central US. In the northern hemisphere, counter-clockwise rotating storms are most common, although clockwise-rotating storms are also produced by the model in lesser numbers. In the southern hemisphere, the opposite is true. The most common direction of thunderstorm rotation is primarily governed not directly by the earth's rotation, but by large-scale weather systems. Specific behavior of individual thunderstorms also controls which way they rotate.

1 Introduction

Thunderstorm updrafts are sometimes observed to rotate. This is well-understood in the context of severe weather in continental convection, especially over the contiguous United States (CONUS), e.g., Kain et al. 2008. More recently the role of vortical hot towers (VHTs; Hendricks et al. 2004, Guimond et al. 2010) in tropical cyclone intensity changes has become better understood. But updraft rotation is typically studied in isolated events, and it has not been considered as a broadly distributed phenomenon. This is in part due to the lack of observations of rotating convection. Indeed, the frequency of strongly rotating updrafts even in the CONUS was underestimated before the installation of a dense nationwide Doppler radar network. Even here the spatial distribution of rotating updrafts has been scarcely studied except as for its role in creating severe weather, specifically supercell thunderstorms and tornadoes. Rotation of sub-severe storms—those not meeting NWS severe weather criteria—has apparently not been studied at all. VHTs are beginning to be observed through geostationary satellites and in some aircraft observations (Hogsett and Stewart 2014) but most effort at understanding these mostly uses regional simulations, and exclusively in the context of mature and intensifying tropical cyclones where there has been some effort to better understand their role in genesis and intensification (Kilroy 2021, and references therein; Wang 2018, and references therein; Zawislak 2020; Hendricks et al. 2004). An appreciation for rotating updrafts elsewhere is virtually absent. Existing global models are too coarse to represent updrafts or their rotation. Regional convective-scale models focus on severe weather and VHTs, and run at most only for a few days, restricting understanding of the patterns of their occurrence, and of interactions between storms or between scales.

Updraft rotation, even if not of severe magnitude, is worth studying as it may provide useful insight into the characteristics of thunderstorms, including their life cycles, mutual interactions, and their dependence upon the larger-scale environment. This would hold true worldwide, not just for mid-latitude severe convection or VHTs, but also for air-mass convection, tropical convective clusters, tropical cyclogenesis, and tropical continental convection. As convective-scale regional models are extending their forecasts into the medium range and global

models approach convection-allowing scales, a better understanding of the behavior of explicit convection and its interactions with larger scales becomes increasingly important. This is especially true as convective parameterizations are disabled in these models, requiring an accurate simulation of multi-day and upscale impacts of explicit convection to properly maintain and predict synoptic and global circulations.

Emerging global storm-resolving models (GSRMs; Satoh et al. 2019) are ideally suited to give a global picture of rotating convection and its interactions with the large-scale environment. Previous research (Miyamoto 2013; Wedi et al. 2020; Seiki et al. 2022; Cheng et al. 2022; and references therein) has made some progress on understanding the properties of global explicit convection but not of rotating convection cells.

In this paper we investigate rotating convection in a year-long GSRM simulation, forced by analyzed sea-surface temperatures, of the GFDL System for High-resolution prediction on Earth-to-Local Domains (SHiELD). This configuration has been submitted to phase 2 of the Dynamics of the Atmospheric general circulation Modeled On Non-hydrostatic Domains initiative (DYAMOND; https://www.esiwace.eu/services/dyamond-initiative/services-dyamond-winter, Stephan et al. 2022). We will find that convection frequently rotates, and that the preferred sense of rotation depends on latitude and on geography, especially over continents. We will also find that environmental shear provides a good estimate for the prevalence of either sense of rotation, but that local storm-scale dynamics still play an important role in the development of rotation. This work is accomplished by taking concepts from severe weather research, developed principally over the CONUS, and applying them worldwide, in combination with analyses typically applied to intraseasonal and longer-timescale variability.

Experimental aircraft developed by the National Aeronautics and Space Administration (NASA) are designated "X-Planes". SHiELD's dynamical core, FV3, was first developed at NASA (Lin and Rood 1996; Putman and Lin 2007), and FV3's creator Shian-Jiann Lin was trained as an aeronautical engineer. In honor of this heritage, we have named this GSRM "X-SHiELD", the eXperimental configuration of SHiELD.

2 Methods

X-SHiELD is a configuration of SHiELD (Harris et al. 2020). We briefly describe the 2021 version used in this paper. X-SHiELD is discretized on a C3072 (3.25-km) cubed-sphere grid with 79 vertical levels, with the lowest mid-level at 10 m above the surface. X-SHiELD couples nonhydrostatic FV3 to physical parameterizations including the 2020 versions of the GFDL microphysics (Zhou et al. 2019, 2022), the prognostic TKE form of the EDMF turbulence scheme (Han and Bretherton, 2019), and the Noah-MP land-surface model with high-resolution fixed files provided by the Environmental Modeling Center. X-SHiELD also uses Scale-Aware SAS (Han et al. 2017) to parameterize shallow convection; there is no deep convective parameterization. There are no inter-

active aerosols, and the only chemistry is stratospheric ozone represented by a simple linear parameterization based on the observed long-term climatology.

X-SHiELD grew out of an earlier GFDL FV3-based GSRM, which was submitted to the first phase of DYAMOND (Stevens et al. 2019) and has been part of earlier evaluations (Judt et al. 2021; Nugent et al. 2022; Turbeville et al. 2022). A 40-day simulation with the 2021 version of X-SHiELD was submitted to the second phase of DYAMOND (Duras et al. 2021) and evaluation is underway (Stephan et al. 2022).

We perform a 15-month integration starting at 00 UTC on 20 October 2019 and ending 00 UTC on 17 January 2021 (455 days) although only dates in 2020 are considered in this manuscript. We use a mixed-layer ocean nudged towards analyzed ECMWF SSTs, per the DYAMOND protocol. A complimentary analysis of this simulation and a companion warmed-climate simulation is described in Cheng et al. (2022).

Convective frequencies are computed using native-resolution output of 6-hr column-maximum updraft velocity (W_{up}) below 100 hPa, and 6-hr extreme values of counter-clockwise (positive) and clockwise (negative) 2-5 km updraft helicity (UH). We define "intense" convection as that for which W_{up} is greater than 10 m s^{-1}. We define

$$\mathrm{UH} = \int_{2\ \mathrm{km}}^{5\ \mathrm{km}} \mathrm{w}\ \ dz,$$

where w is the vertical velocity and ς is the relative vertical vorticity. This quantity is a frequently used proxy for severe weather in convective-scale prediction models (Droegemeier et al. 1993; Kain et al. 2008). Typically, thresholds of 50 to 250 m^2 s^{-2} are used to indicate potentially severe weather events, but this threshold is model-dependent. In FV3, both vertical velocity and vertical vorticity are grid-cell mean quantities and so UH can be computed exactly, leading to larger values in FV3-based models than those using other dynamical cores (Potvin et al. 2019). The threshold used by the Storm Prediction Center to indicate CONUS severe weather in FV3-based convective-scale models is 250 m^2 s^{-2}, corresponding to the 99.85 percentile of hourly-maximum UH values during the peak of severe weather season in May (about 1 out of 650 grid columns; see https://www.spc.noaa.gov/exper/href). These intense UH values are very rare worldwide, as we will see below; this study principally examines UH values smaller than this as our focus is on rotating convection overall and not merely the most extreme events. Note further that the maximum vertical velocity in a deep, intense updraft will be attained in the upper troposphere, well above the 2-5 km layer in which UH is computed. Thus, the magnitude of W_{up} is not the vertical velocity that is used to compute UH, which even in severe thunderstorms will be much lower.

Counts of 6-hr threshold values of both W_{up} and UH are accumulated into

0.75 x 0.75-degree bins for display and calculation (roughly equal to the 80-km grid bins used for validation of severe storm forecasts; cf. Sobash et al. 2011, Hitchens et al. 2013). Counts are of individual grid columns and not convective objects and represent the *average* number of seasonal or annual events at any point within a bin. Analysis is restricted to areas below 60° latitude in both hemispheres, poleward of which convection is rare.

3 Results

3.1 *Global distribution of intense and rotating convection*

The global distribution and annual cycle of deep convection is well understood (Liu and Zipser 2005; Houze et al. 2015). We see in Figure 1 that intense convection in X-SHiELD is most common over the deep tropics year-round and follows the migration of the ITCZ. Intense convection is also present in the extratropical storm tracks and in common tropical cyclone paths, and in the South Pacific Convergence Zone. We also see frequent intense convection in the warm seasons over mid-latitude continents, most notably over the central United States but also in northern Eurasia, central China, Argentina, southern Africa, and Australia. Note the large areas in the subtropics, especially in the southern hemisphere, where convection is absent. Convection is also nearly absent over the ocean poleward of 40° latitude. These results are in line with the observed frequency of intense convection as defined from satellite-based radar reflectivity (Liu et al. 2007, Houze et al. 2015) and give confidence that X-SHiELD is producing a realistic frequency of intense convection.

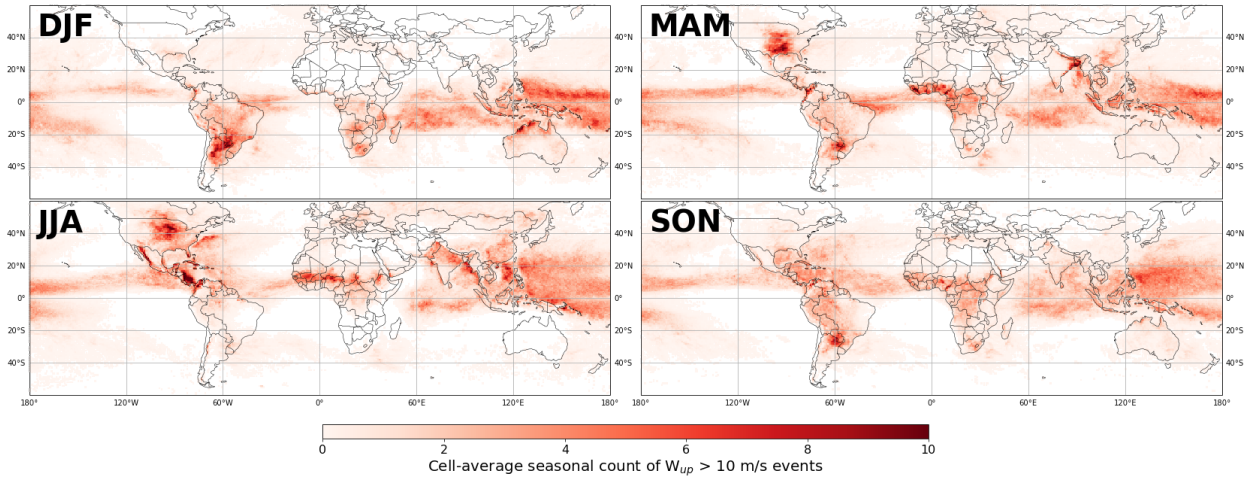

Figure 1. Seasonal 0.75-by-0.75-degree bin-mean count of intense convection events, (W_{up} >10 m s^{-1}). White represents bins with no events in a season.

The spatial distribution of rotating updrafts largely follows that of convective updrafts, although the sense of rotation shows a more complex pattern. Figure 2 shows the frequency of which UH magnitude is greater than 50 m^2 s^{-2} for both positive (counter-clockwise) and negative (clockwise) values. This is a small

threshold compared to traditional thresholds used for CONUS severe weather prediction and especially for FV3-based convective-scale models which produce very high values of UH (Potvin et al. 2019) but is useful for detecting storm rotation especially in the lower latitudes where environmental sources of vertical vorticity are weak.

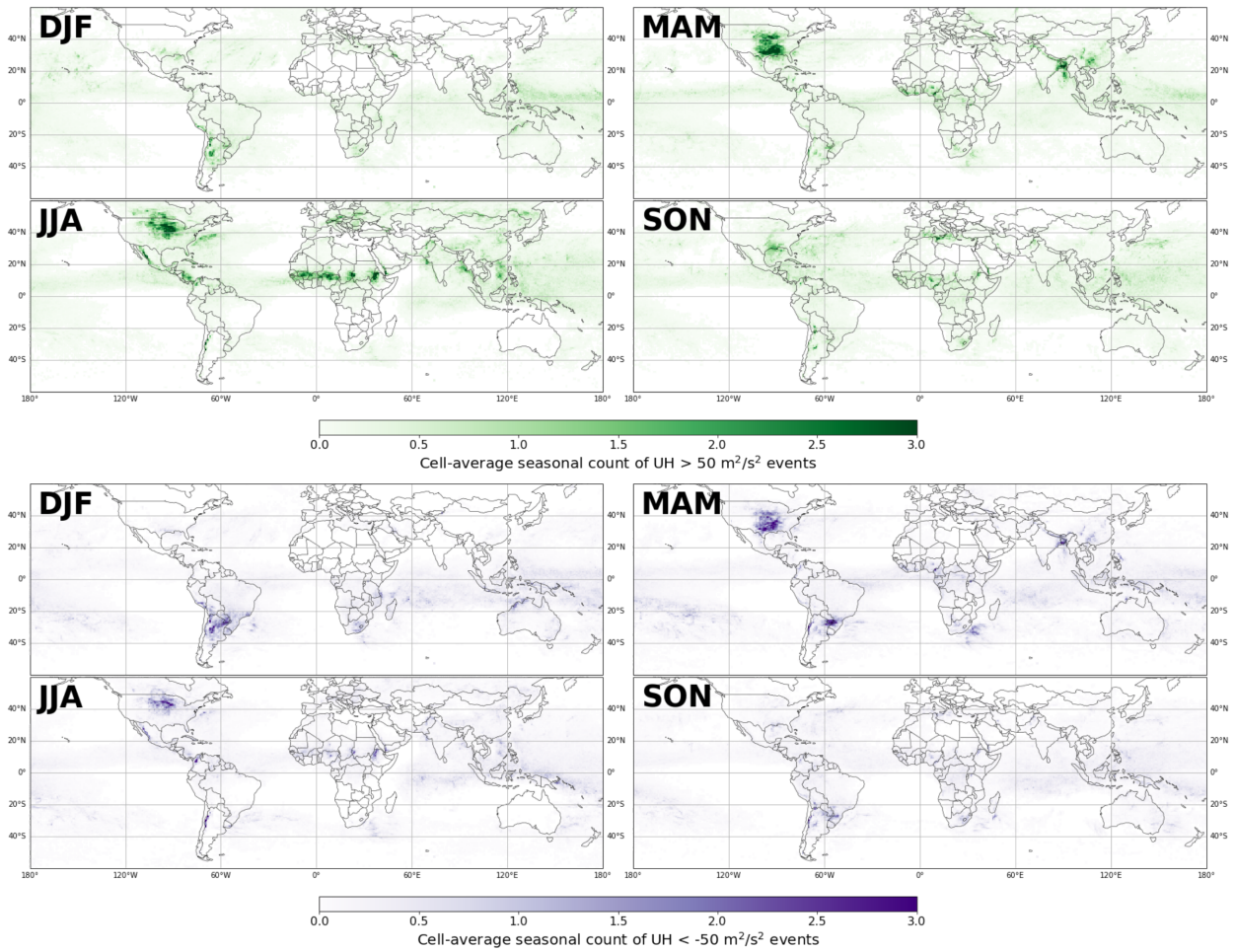

Figure 2. As in Figure 1, except for UH magnitudes larger than 50 m^2 s^{-2}: top, positive (counter-clockwise rotating) events; bottom, negative (clockwise-rotating) events.

It is readily apparent that the cyclonic sign of UH (positive in the northern hemisphere, negative in the southern hemisphere) dominates away from the equator, especially over the ocean; this signature is weaker over the continents. We quantify this in Figure 3: yellow regions correspond to areas in which cyclonic updrafts are at least four times as frequent as anticyclonic, while purple indicates a closer equality of the two orientations. Anticyclonic updrafts pre-

dominate only in small regions along the equator, where 'cyclonic' has little meaning; along the peaks of mountain ranges, where local effects may prefer one sign of rotation; and in some areas of very few convective events. In the high northern latitudes cyclonic updrafts are several times more frequent than anticyclonic, although this represents a small number of events.

Clearly, except in the deep tropics, oceanic convection is preferentially cyclonically rotating. In continental convective hot spots cyclonic updrafts still tend to be more frequent, but there are also significant numbers of anticyclonic updrafts. This correspondence is by no means universal and there are interesting geographic and seasonal variations seen in Figure 2, such as a greater preference for cyclonic rotation in the cold seasons (SON, DJF) in the Eastern Pacific between Mexico and Peru, and in the Gulf of Mexico and Southeastern US. The seasonal cycle of this ratio over the Indian Subcontinent is also unusual: in the monsoon season (JJA) and into SON the convection is more oceanic in nature, with a distinct cyclonic preference, but in MAM there is no such preference.

How frequently do intense updrafts rotate? Figure 4 shows the fraction of $W_{up} > 10$ m s^{-1} updrafts that meet the 50 m^2 s^{-2} UH criterion, in either sense of rotation. While not all updrafts rotate to an appreciable degree, in nearly all convective regions at least some fraction do. In general, rotation is more frequent in the subtropics and mid-latitudes, where about half of all intense updrafts also meet this UH threshold. While it is possible for non-intense updrafts to exhibit sufficient rotation to meet this threshold, we disregard these as being less important for our analysis.

For UH values meeting the Storm Prediction Center's severe threshold for FV3-based models (250 m^2 s^{-2}) many of the aforementioned features are even more clear (Figure 5). Positive severe UH dominates in the northern hemisphere and negative severe UH dominates in the southern hemisphere. As we expect, most severe UH events occur over land, and the few events occurring over the ocean are overwhelmingly cyclonic. Larger counts of severe UH correspond to the warm seasons of the central United States, Argentina, South Africa, sub-Saharan Africa, the Bay of Bengal, and in a band from central Europe into eastern Siberia. Anticyclonic severe updrafts are rare, especially over the ocean, and in the locations where they do occur with any frequency (CONUS, Bay of Bengal, South America) they are still much less common than cyclonic severe updrafts.

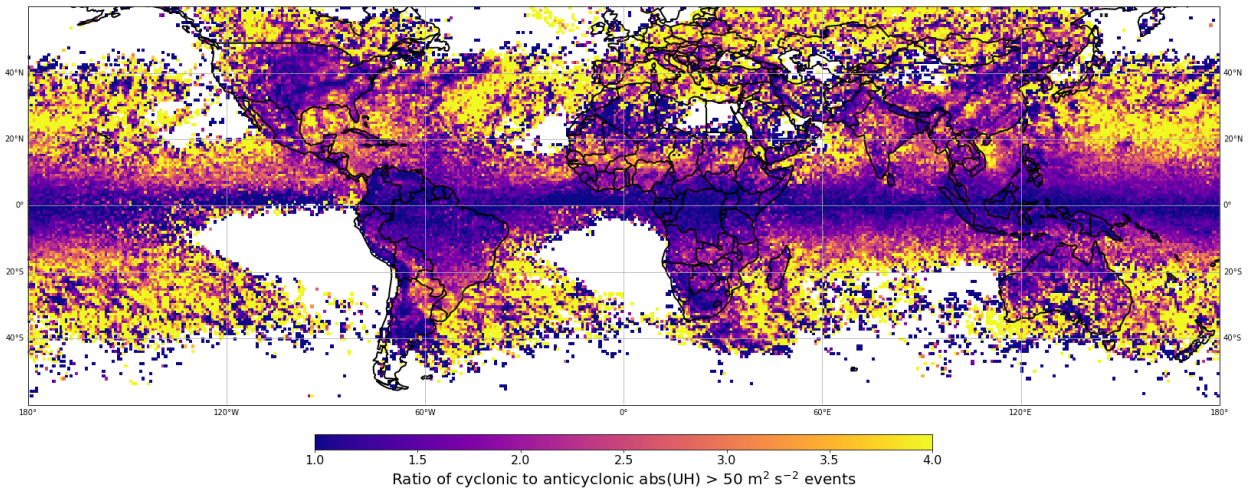

Figure 3. Annual ratio of cyclonic to anticyclonic UH events of magnitude > 50 m^2 s^{-2} events. White regions represent areas without UH events above this threshold.

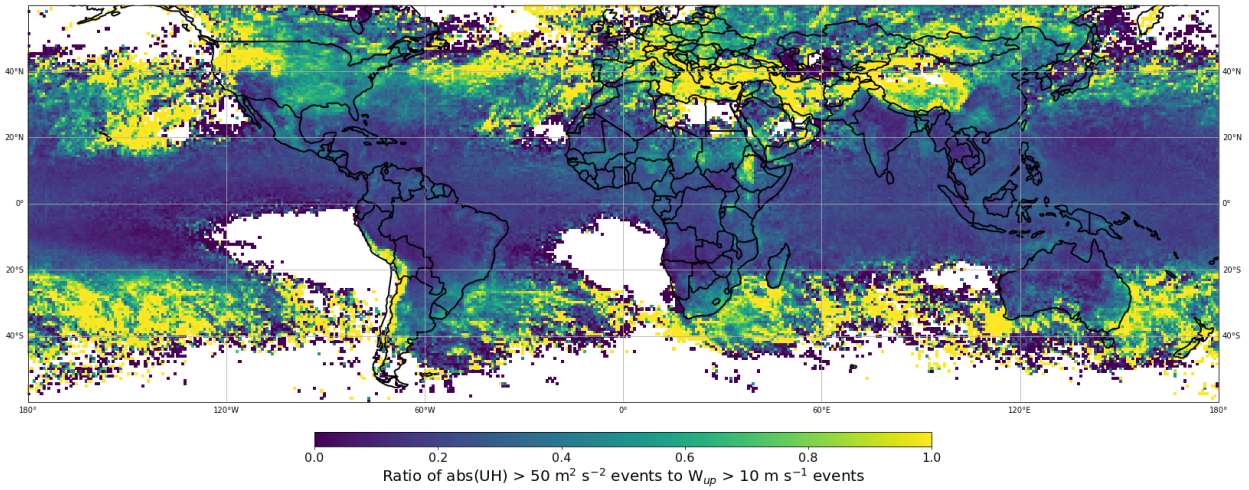

Figure 4. Annual fraction of intense updrafts which rotate (ratio of abs(UH) > 50 m^2 s^{-2} to W_{up} > 10 m s^{-1}).

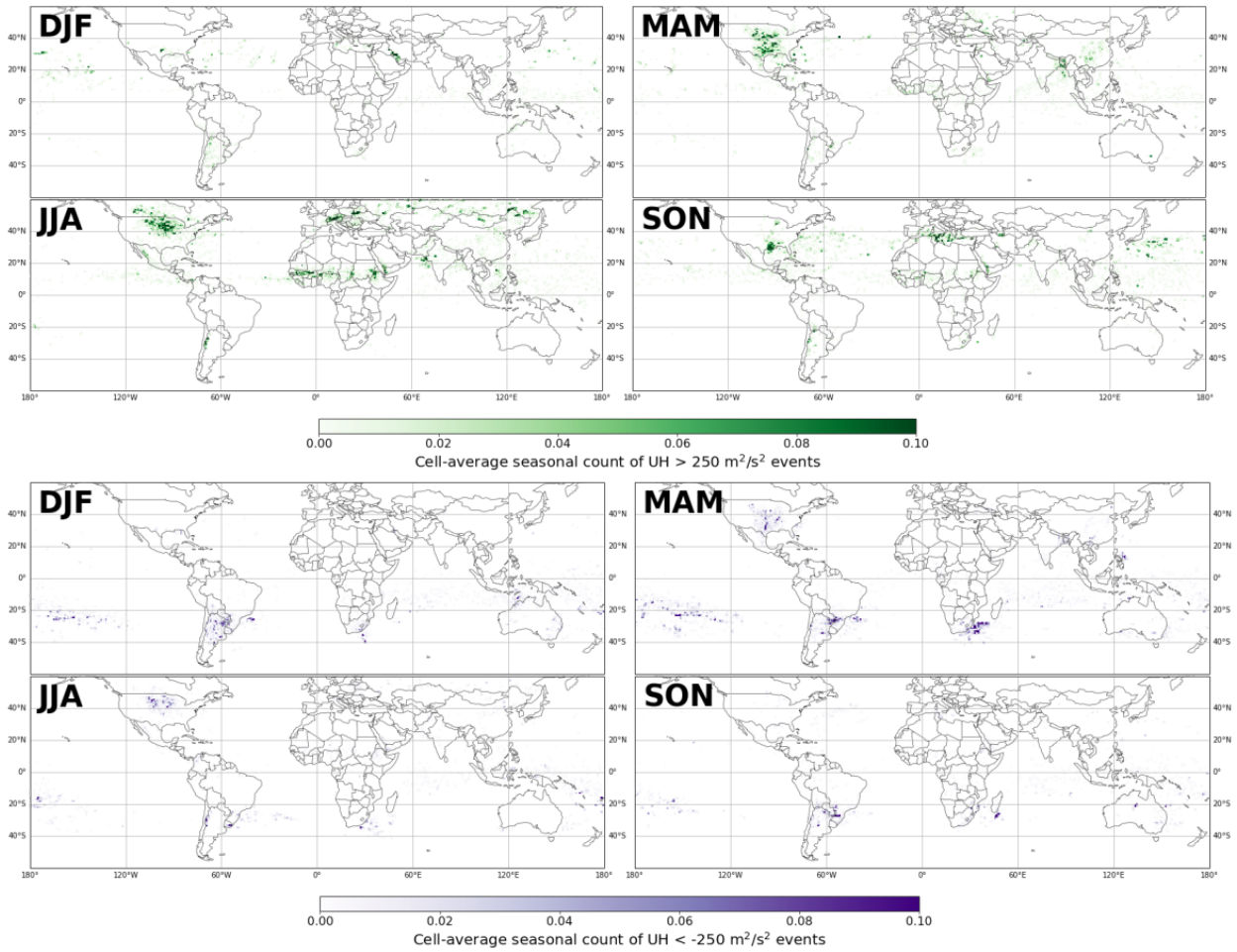

Figure 5. As in Figure 2, but for a 250 m^2 s^{-2} threshold.

3.2 Validation of convection and rotation

Precipitation provides an adequate means of validating how well the model represents convection globally. X-SHiELD well reproduces 2020's precipitation observation from the Global Precipitation Measurement satellite (GPM; Huffman et al. 2019) with global root mean square errors (RMSE) of only about 1.2 mm/day (Figure 6). This compares well with CMIP6 climate models (cf. Boucher et al. 2020; Zhao et al. 2018), despite X-SHiELD only having a single year's simulation to be validated. X-SHiELD has a global average precipitation of 2.9 mm/day compared to the GPM estimate of 2.7 mm/day, although observational and reanalysis datasets disagree on the global average precipitation rate and the precise value remains elusive (Gehne et al. 2016). X-SHiELD tends to have too much precipitation in the tropical convective regions and too little in the extratropical storm tracks. Areas of lighter precipitation are also broader

than in GPM, possibly due to an excess of light precipitation in X-SHiELD.

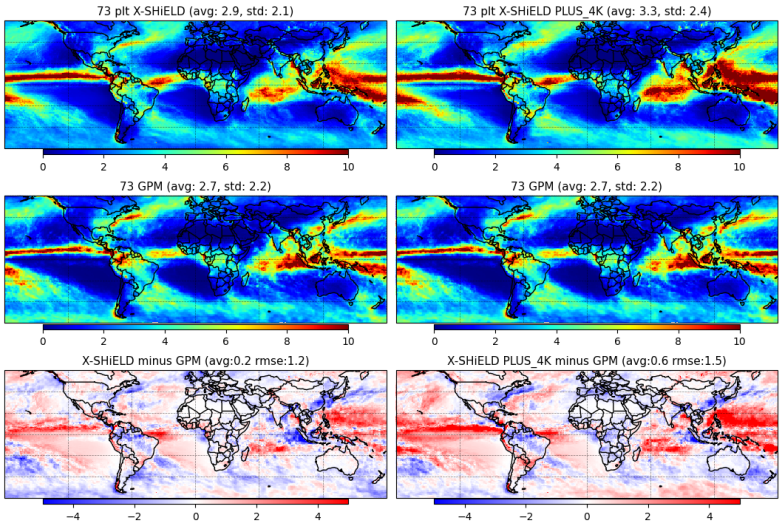

Figure 6. Year-mean precipitation (mm d^{-1}) compared to the Global Precipitation Measurement observation for 2020. Numbers in panel titles represent the average ("avg"), standard deviation ("std") and root-mean square error ("rmse") for the GPM domain of 60° S to 60° N latitude.

Worldwide observations of rotating convection do not exist making it challenging to validate the distribution thereof. Over the CONUS simulated UH values above a certain threshold are considered proxies for severe weather and so severe weather reports (tornadoes, strong winds, large hail) are used as a validation dataset (cf. Sobash et al. 2011, Hitchens et al. 2013). Here, we take 2020 tornado reports from the Storm Events Database (https://www.ncdc.noaa.gov/stormevents/) and following the methodology of Sobash et al., sort daily events into 0.75-by-0.75 degree bins. Under this methodology, a 'hit' is when there is at least one event—either a simulated UH magnitude over the threshold or a tornado report—within a bin. The resulting grid is then smoothed using a Gaussian filter.

Considering that there is not a direct mapping between simulated storm rotation and a real-world tornado report, and that only about 1 in 4 mesocyclones (intense rotating thunderstorms) produce tornadoes (Trapp et al. 2005), there is still considerable similarity in the pattern of severe rotation days (Figure 7a, both senses of rotation) and reported tornado days (Figure 7b). The two maxima seen in the UH frequencies, one centered over Iowa, the other over Louisiana and Texas, separated by a local minimum from central Oklahoma into Illinois, bears a striking although likely coincidental resemblance to the pattern of tornado reports in 2020, with maxima in northern Illinois and in southern Mississippi. This result gives us some confidence that X-SHiELD is simulating UH frequencies reasonably well, to the limitations of our one year of

simulation and its less-than-optimal compatibility with the available validation dataset. However, the observed higher frequency of tornadoes in the Southeastern US, along the front range of the Rocky Mountains, and along the US Atlantic Coast, is not reflected in the simulated UH frequency. X-SHiELD also produces significant counts of severe rotation days in the high northern Plains, especially in sparsely populated western Nebraska and South Dakota, which is not supported by the storm reports. It is also evident from the top two panels of Figure 7 again that while cyclonic (positive) UH predominates, anticyclonic UH is not uncommon especially in the upper midwestern states.

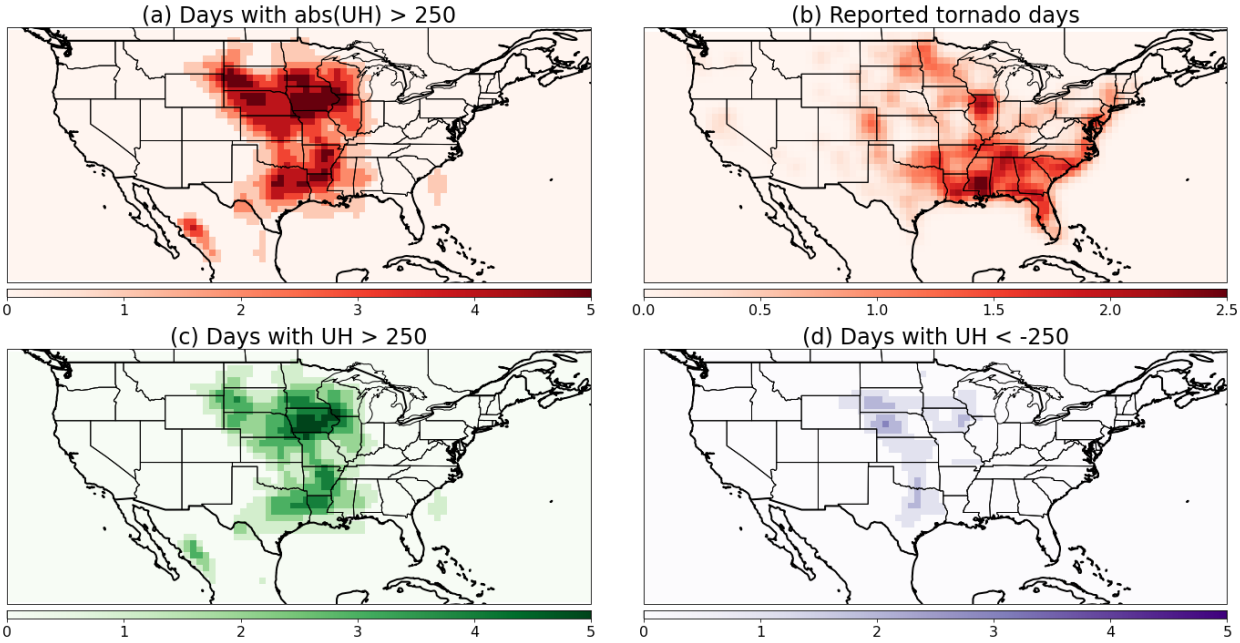

Figure 7. CONUS number of days with severe UH or a reported tornado in 2020. See text for methodology. The colorbar for observed tornado days in (b) differs from the others reflecting the small fraction of rotating storms that cause tornadoes (Trapp et al. 2005).

3.3 Quantification of global convection and rotation

To quantify our qualitative senses of updraft rotation, Figure 8 shows the ratios of the zonal mean frequencies of positive vs. negative UH, for the ocean and separately for the continents in both the western and eastern hemispheres. The zonal means validate the qualitative patterns deduced from Figure 2: over the ocean cyclonic rotation dominates and increases poleward until about 20–30° latitude. This corresponds to regions in which tropical cyclogenesis is common, which are virtually all cyclonic. Over the land the pattern is more complex as this monotonic increase is only seen in the deep tropics equatorward of 10° latitude, with local minima in the ratio in the mid latitudes corresponding to convective hot spots: the central US and Argentina in the western hemisphere,

and in west Africa, South Africa, Australia, and central across Eurasia in the eastern hemisphere.

In all regions this behavior is reproduced for increasingly high UH thresholds, and nearly universally the ratios increase with increasing threshold. These relations hold all the way up to 200 m^2 s^{-2}, nearing the model's threshold for severe weather. At this 200 m^2 s^{-2} magnitude the relationships become even more striking, notwithstanding the additional noisiness in the plot due to the relatively small number of events (Supplemental Figure 1).

Continental hot spots show a smaller but still distinct preference for cyclonically rotating updrafts. This is especially true for strong storms with UH thresholds of 200 m^2 s^{-2}, for which cyclonically-rotating updrafts are 3–5 times more frequent than anticyclonic updrafts. This is in line with the typical CONUS experience that severe storms are most frequently cyclonically-rotating, as was also seen for 250 m^2 s^{-2} in Figure 5.

We plot probability distribution functions (PDFs) of the UH in Figure 9 in regions and latitude bands to better quantify the relative frequencies of each sense of rotation. Here we show only UH for intense convection, so that the results are not dominated by weak updrafts. Over the ocean in both hemispheres there is a greater preference for cyclonic UH that increases in more poleward latitudes and with UH threshold; there are also more total events counted at lower latitudes over the ocean. The PDFs over land are more complex but the same broad pattern is seen. Intriguingly, nearly all the curves meet at a certain crossover point, about 25 m^2 s^{-2}. This may indicate that 25 m^2 s^{-2} is the lowest UH value which is scientifically meaningful even though this includes values representing sub-severe convection.

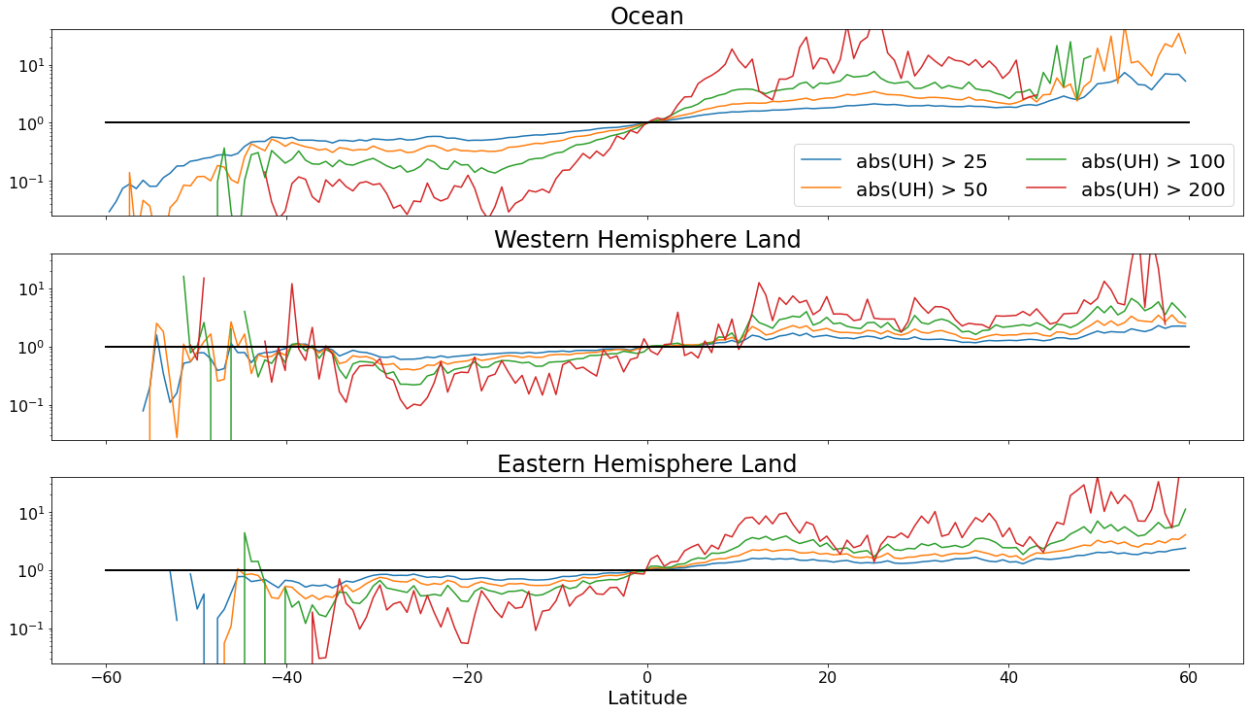

Figure 8. Zonal-mean annual relative counts of positive to negative UH events of different magnitudes over the ocean (top), western-hemisphere land (WH: North and South America, middle), and eastern-hemisphere land (EH: Africa, Eurasia, Australia, and Maritime Continent, bottom). Count ratios in each 0.75° latitude band are plotted on a log scale. Supplemental Figure 1 shows absolute counts of both senses of rotation.

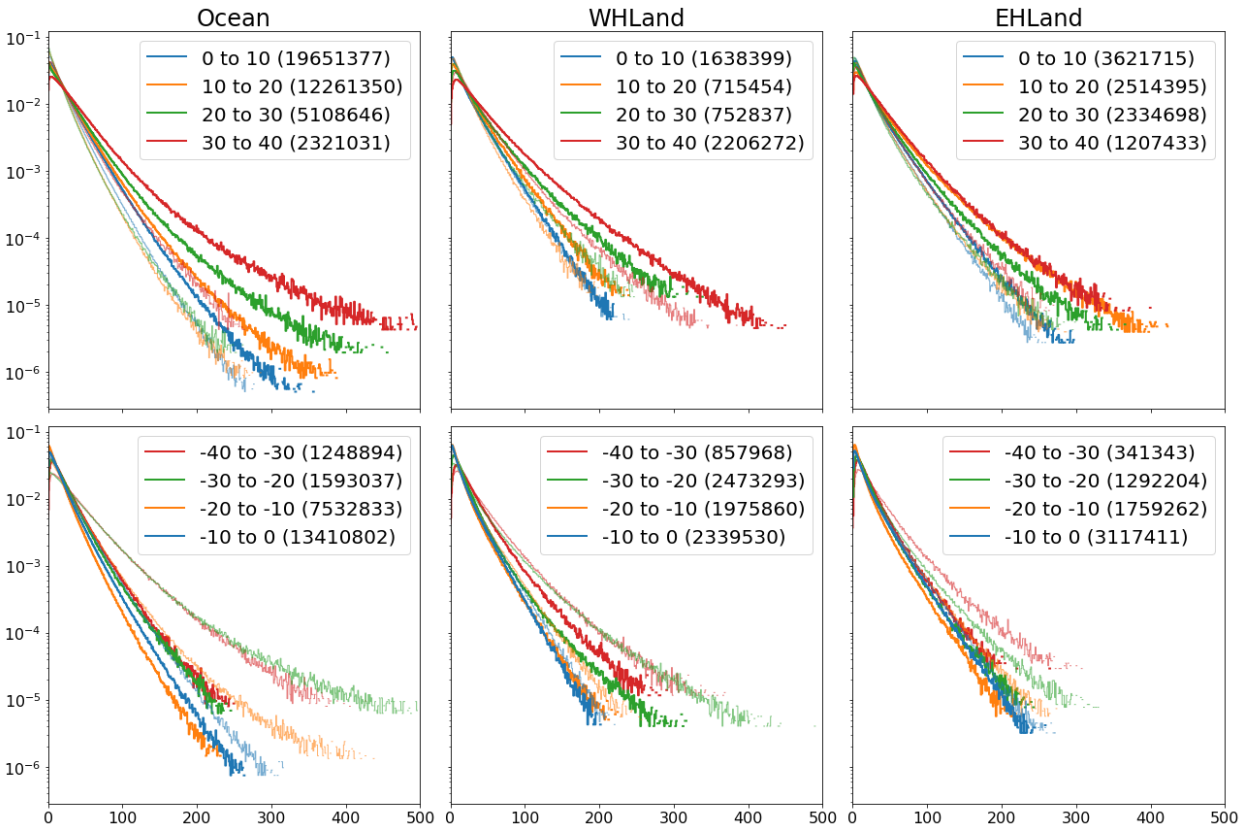

Figure 9. Conditional probability distribution functions of positive (heavy lines) and negative (light, thin lines) UH for intense convection (grid cells in which $W_{up} > 10$ m s^{-1}) in different regions (as in Figure 8) and latitude bands. Normalization is by the number of cells with intense convection, given in parentheses in the legends. UH bins with fewer than 10 events are not plotted.

3.4 Example: rotating convection in the tropical western Pacific

We can deduce some facts about the origins of rotation in convective updrafts from these ratios. Since the timescale of convective updrafts is short, we cannot ascribe their sense of rotation directly to the convergence of planetary vorticity, although this has an indirect effect on convection through synoptic-scale systems that give preference to one sign of rotation or the creation of horizontal shear zones that affect updrafts. This inference does not rule out convergence of relative vorticity as the origin of rotating updrafts.

The JJA tropical Pacific provides an illustration of these processes (Figure 10). In both the deep tropics and subtropics, rotating updrafts are associated with propagating convective clusters (indicated by low OLR values). In the subtropics (20–30 N) cyclonic updrafts are usually several times more frequent than anticyclonic updrafts, although we find at this threshold (50 m^2 s^{-2}) that the

events with the most frequent cyclonic updrafts are co-located with significant numbers of anticyclonic updrafts. In these events the ratio is much closer to unity (and in some cases anticyclonic rotation dominates) than in the events for which fewer rotating updrafts are present. An analysis with a larger 100 m^2 s^{-2} threshold (Supplemental Figure 2) however reveals that stronger rotation is dominated by cyclonic rotation, with only a small number of events in which strong anticyclonic rotation dominates. This gives an indication that significant numbers of updrafts with both senses of rotation are created, but that the anticyclonically-rotating updrafts are weaker. We will return to this point below. Meanwhile, in the deep tropics (0–10 N) there are roughly equal numbers of both signs of UH. The patterns of cyclonic and anticyclonic frequencies are very similar indicating the same processes are giving rise to both senses.

We can quantify these suppositions by looking at the probability distribution functions of either sign of UH in intense convection. In this region and in these months, the frequency of cyclonic updrafts is roughly the same for all thresholds in the deep tropics and over 10 to 20°N latitude, with slightly less in the subtropics (Figure 11, left). However, the frequency of anticyclonic updrafts clearly decreases in the more poleward bands, and the frequency relative to the number of cyclonic updrafts decreases with threshold, to the point that in the subtropics, an appreciable number of UH $>$ 150 m^2 s^{-2} updrafts are counted but UH $<$ -150 m^2 s^{-2} is very rare. Again, the crossover of the curves in both panels is at about 25 m^2 s^{-2}, lending credence to our hypothesis that this is the minimal meaningful value of UH.

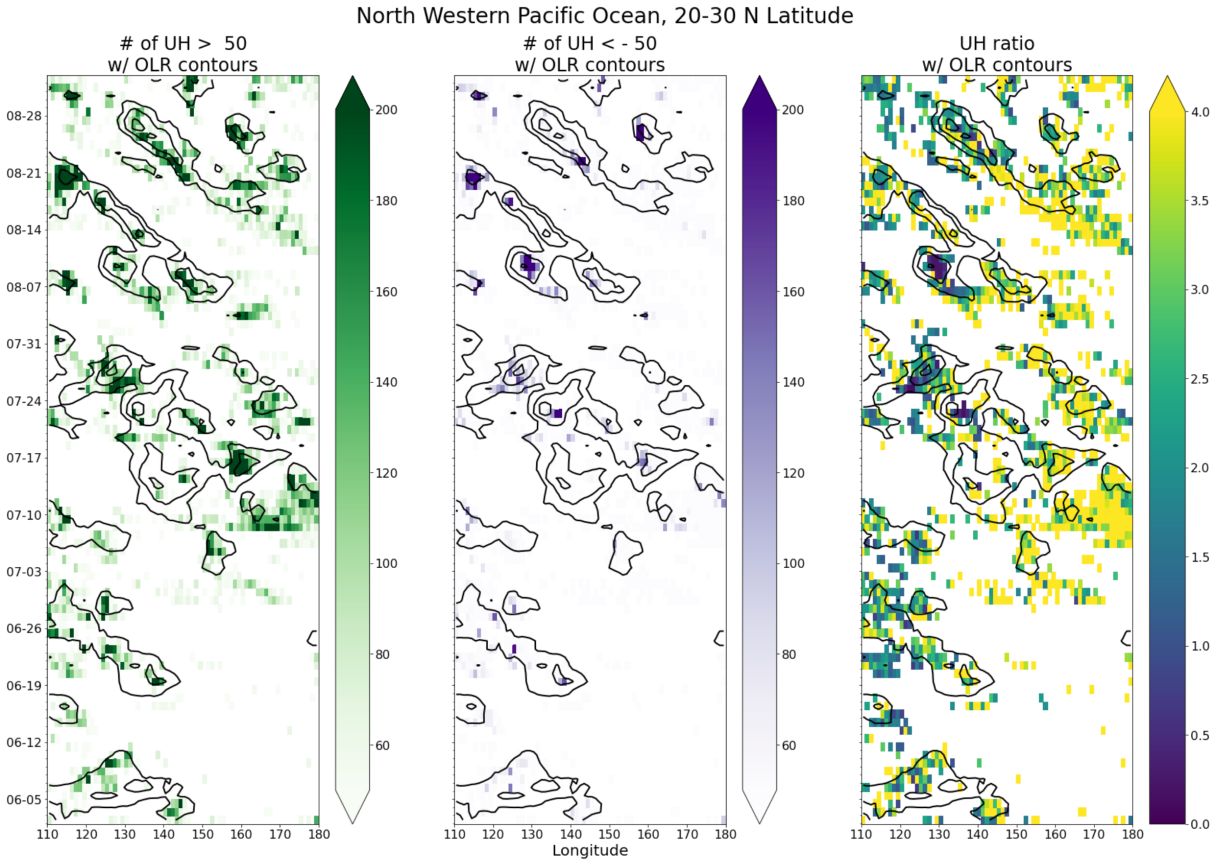
North Western Pacific Ocean, 20-30 N Latitude
# of UH > 50
w/ OLR contours
# of UH < - 50
w/ OLR contours
UH ratio
w/ OLR contours
08-28
08-21
08-14
08-07
07-31
07-24
07-17
07-10
07-03
06-26
06-19
06-12
06-05
110 120 130 140 150 160 170 180
Longitude
200
180
160
140
120
100
80
60
4.0
3.5
3.0
2.5
2.0
1.5
1.0
0.5
0.0

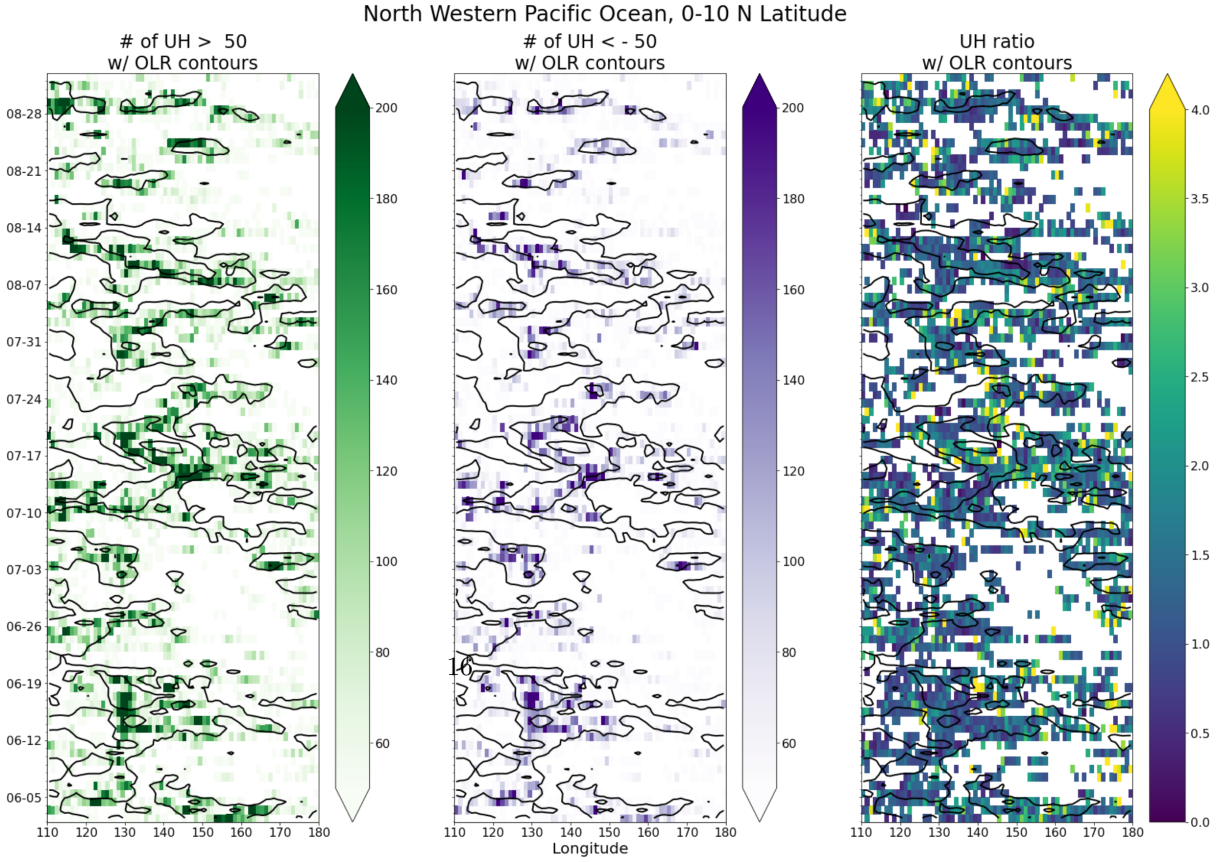
North Western Pacific Ocean, 0-10 N Latitude
# of UH > 50
w/ OLR contours
# of UH < - 50
w/ OLR contours
UH ratio
w/ OLR contours
08-28
08-21
08-14
08-07
07-31
07-24
07-17
07-10
07-03
06-26
06-19
06-12
06-05
110 120 130 140 150 160 170 180
Longitude
200
180
160
140
120
100
80
60
4.0
3.5
3.0
2.5
2.0
1.5
1.0
0.5
0.0

Figure 10 (previous page). Hovmuller (time-longitude) plots averaged within two latitude bands in the Western Pacific for JJA. Shaded colors are counts in 1-degree longitude bins of daily UH > 50 m2 s-2 events for positive (left) and negative (center) UH values; the shading in the right panel is the ratio of positive to negative events. Only bins with at least 50 columns per day exceeding the UH thresholds are shown. Black contours represent 100 to 220 W m-2 values of latitudinally-averaged outgoing longwave radiation with a 40 W m-2 contour interval.

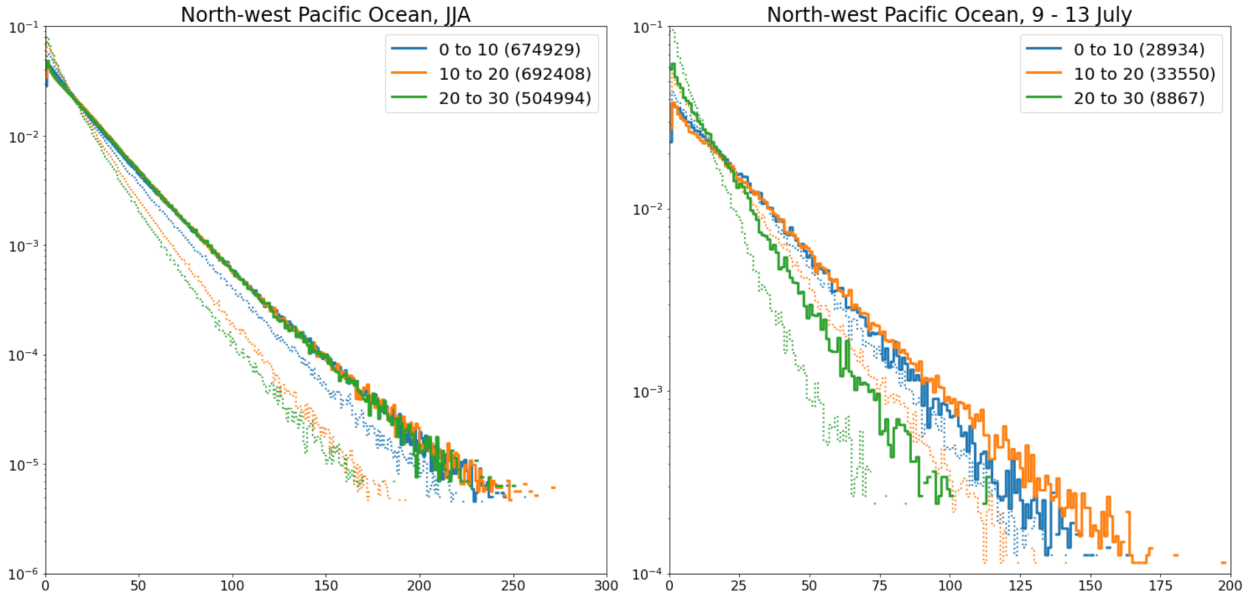

Figure 11. (left) Conditional PDFs over latitude bands (°N) of UH (m^2 s^{-2}, positive solid, negative dotted) in intense updrafts for the region and time period shown in Figure 10. (right) Same but for the region shown in Figure 12. Normalization is by the number of cells with intense convection. Numbers in parens are the count of total events with UH magnitude greater than 25 m^2 s^{-2}. Bins with fewer than 10 events are not plotted. Note different scales on the two panels.

The distinctly enhanced preference for cyclonic rotation in the subtropics suggests that there is an environmental control at work in the generation of rotating convection, even if for individual events local vorticity generation of both signs is still active. This is identifiable from an examination of a pair of cloud clusters in the tropical north-western Pacific for a four-day period in July 2020 (Figure 12). In the cluster in the north-eastern part of the domain, an incipient tropical cyclone, positive UH dominates (blue), whereas there are more negative UH (red) and there is a closer balance between the two signs for the storms close to the coast of Vietnam in the west. The numbers are nearly equal in the cluster in the southeast. This relation is quantified by the PDF in Figure 11 (right) which shows nearly equal frequencies of both senses of rotating updrafts up to

about 125 m^2 s^{-2} in the deep tropics, but many more cyclonic updrafts at higher latitudes. Note that this period is dominated by these three events and has large quiescent regions (especially in the subtropics) and so the PDFs of this region do not match those for the full summer (Figure 11, left) or full year (Figure 9).

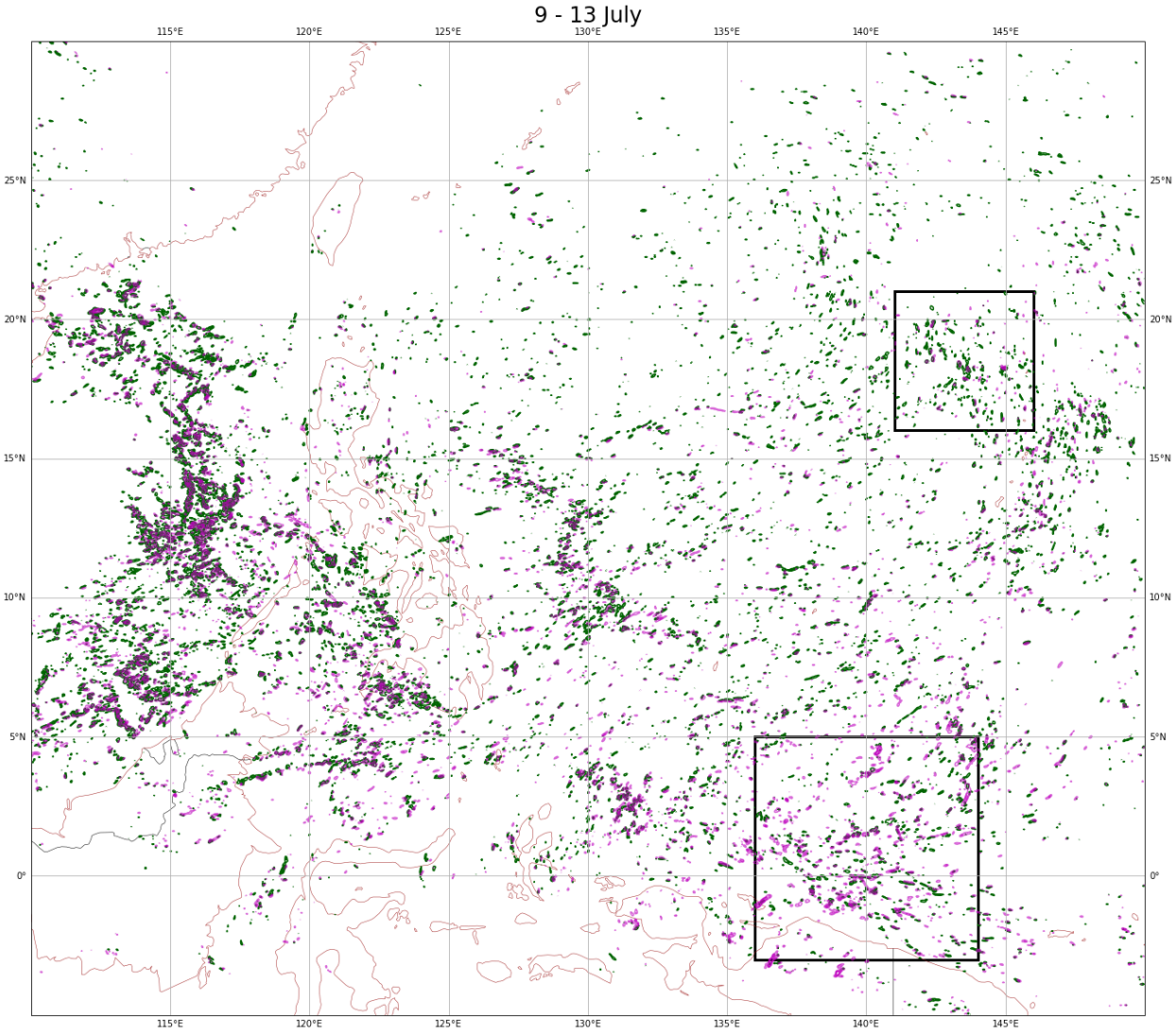

Figure 12. Period-extreme values of positive (green) and negative (purple) UH over the tropical Northwestern Pacific, over a four-day period in July 2020. Contour interval is 50 m^2 s^{-2}. Negative contours are semi-transparent and plotted over positive contours. Regions inside the boxes are shown in Figure 13.

By zooming in on the clusters (Figure 13) we can get a better sense of the be-

havior of convective cells. In the subtropical cluster (Figure 13, top) numerous updraft tracks are seen, many of which overlap over the 48-hour period and not all of which are associated with strong rotation. In many cases those that do rotate show pairs of positive and negative UH, a signature of baroclinically-generated vorticity tilted into the vertical. This is strong evidence that the vertical vorticity is created in-situ and not necessarily directly from the convergence of planetary rotation; the short tracks of convective cells suggest that their lifetimes are too short for this effect to be significant. These pairs can be compared to vorticity dipoles seen in the idealized simulations of Kilroy and Smith (2015, 2016). Note that in this region the prevailing flow is northerly as part of the cluster's circulation, and so the cyclonic right-moving cell usually is to the west of the anticyclonic left-moving cell.

While large (UH > 100 m^2 s^{-2}) values of both signs are present in the subtropical cluster, so that the circumstances leading to individual storm formation are important for the sense of rotation and how large the UH gets, it is apparent from Figure 13 (top) that positive UH dominates. As was seen in Figure 10, subtropical events with many rotating updrafts tend to have both senses of rotation present, although the cyclonically rotating updrafts have larger UH. This again suggests the action of the local vorticity generation creating counter-rotating updraft pairs, with the cyclonic sense of vorticity being preferred. In the lower-latitude cluster (Figure 13, bottom) pairs of counter-rotating cells are again seen, although the vorticity couplets are less well-organized, and much more negative UH is present than in the subtropical cluster. Since planetary vorticity is so small at this latitude and the convective cell lifetime so short, we can conclude that the preference for one sign of rotation arises from the synoptic environment.

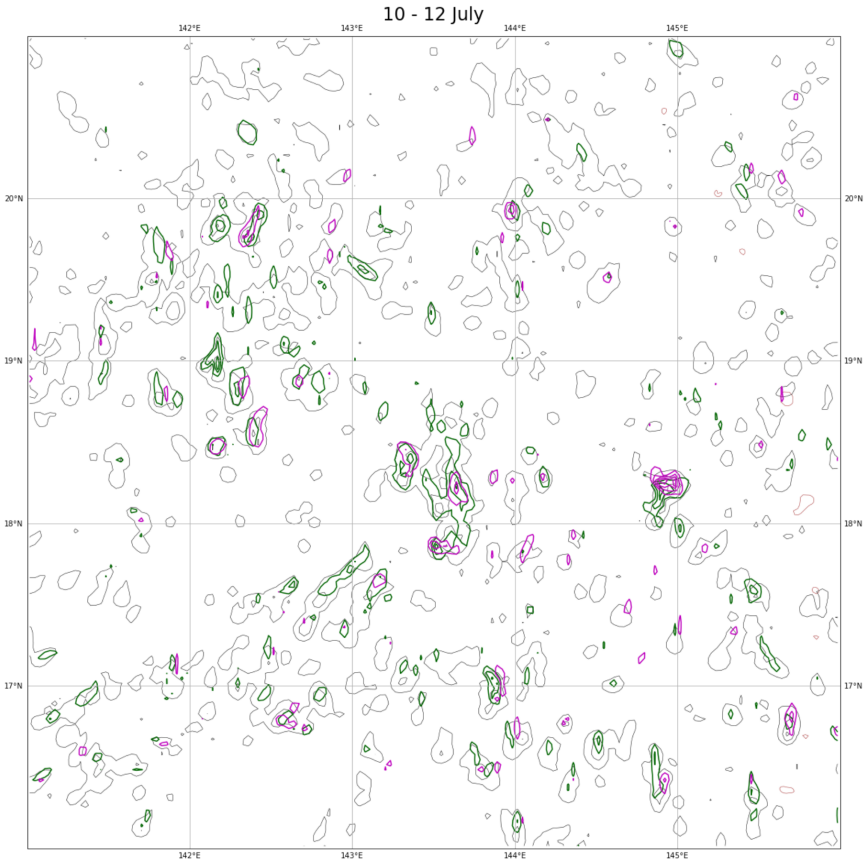
10 - 12 July
142°E
143°E
144°E
145°E
20°N
19°N
18°N
17°N

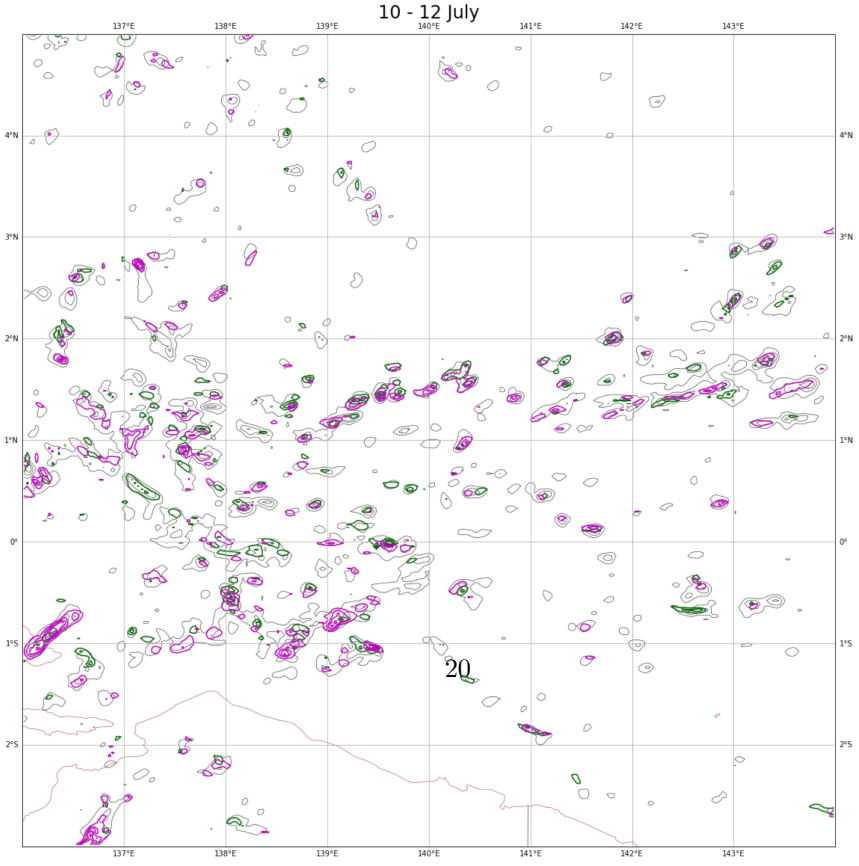
10 - 12 July
137°E
138°E
139°E
140°E
141°E
142°E
143°E
4°N
3°N
2°N
1°N
0°
1°S
2°S

Figure 13 (previous page). As in Figure 12 but zoomed-in over the subtropical (top) and deep tropical (bottom) convective clusters and over a two-day period. Gray contours are period-maximum column-maximum updrafts with a contour interval of 10 m s^{-1}. Note the spatial scale in the two panels is different.

3.5 Role of environmental controls in rotating convection

We have suggested that the environmental vertical wind shear is an important if not the only factor in determining the ratios of cyclonic and anticyclonic updrafts. Figure 14 shows yearly, zonal averages of 0–3 km Storm Relative Helicity (SRH) for the right- and left- moving storms, called R-SRH and L-SRH respectively using the definitions from Bunkers et al. (2000) and Bunkers (2002). Here, we show both the mean weighted by counts of updrafts with max vertical velocity above 10 m s^{-1}, and the unweighted mean. The weighted mean removes the effects of intense cold-season mid-latitude cyclones—in which strongly deformational flows can create SRH values above 1000 m^2 s^{-2}—with little convection as well as quiescent periods also with little convective activity while emphasizing convective outbreaks. Here again, in the northern hemisphere we refer to R-SRH as cyclonic and L-SRH as anticyclonic, with the convention reversed in the southern hemisphere.

There is a striking resemblance with Figure 8: the two senses of SRH are roughly equal at the equator and in the deep tropics, with the cyclonic sense becoming increasingly dominant steadily into the subtropics and mid-latitudes in both hemispheres. The difference in the means is modest in the subtropics, especially in the oceanic subtropics compared to the huge difference between the two orientations in the mid-latitude storm tracks but should be sufficient to cause the simulated preference for cyclonic updrafts. Notably, Eastern Hemisphere continental SRH differences show a close match to the pattern of cyclonic updraft preference: maxima in the ratios towards cyclonic updrafts at 15 and 35 °N and minima at 25 °N and 30 °S closely match similar maxima and minima in differences between cyclonic and anticyclonic SRH. In the continental Western Hemisphere, there is distinctly more cyclonic SRH poleward of 25 degrees latitude, corresponding to the larger numbers of cyclonic updrafts in the mid-latitudes. This correspondence is not perfect: despite the distinct preference for cyclonic updrafts in the western hemisphere's continental subtropics, there is almost no difference between the two senses of SRH in the weighted-mean. Other processes may be at work in these regions.

Although the magnitude of the SRH difference in the mid-latitudes, especially over land, is significantly larger than the SRH difference in the subtropical oceans, this does not correspond to a larger preference for cyclonic updrafts. Indeed, in the subtropical oceans the preference for cyclonic updrafts is significantly larger than in the continental mid-latitudes, much more than can be expected from the SRH difference alone. This points to the well-recognized (cf. Emanuel et al 1989) and fundamental distinction between tropical and mid-latitude convection, in which mid-latitude convection is typically longer-lived and more intense than that in the tropics and is supported by much larger

CAPE and convective inhibition values. It is perhaps that mid-latitude continental convection's strong reliance upon cold pools for its maintenance makes it much more likely that baroclinic vorticity generation is at work, which in some circumstances can generate more anticyclonic updrafts than would be expected from environmental shear parameters alone (Bunkers 2002). It is also possible that local geographic features over land can modify the preference for cyclonic updrafts.

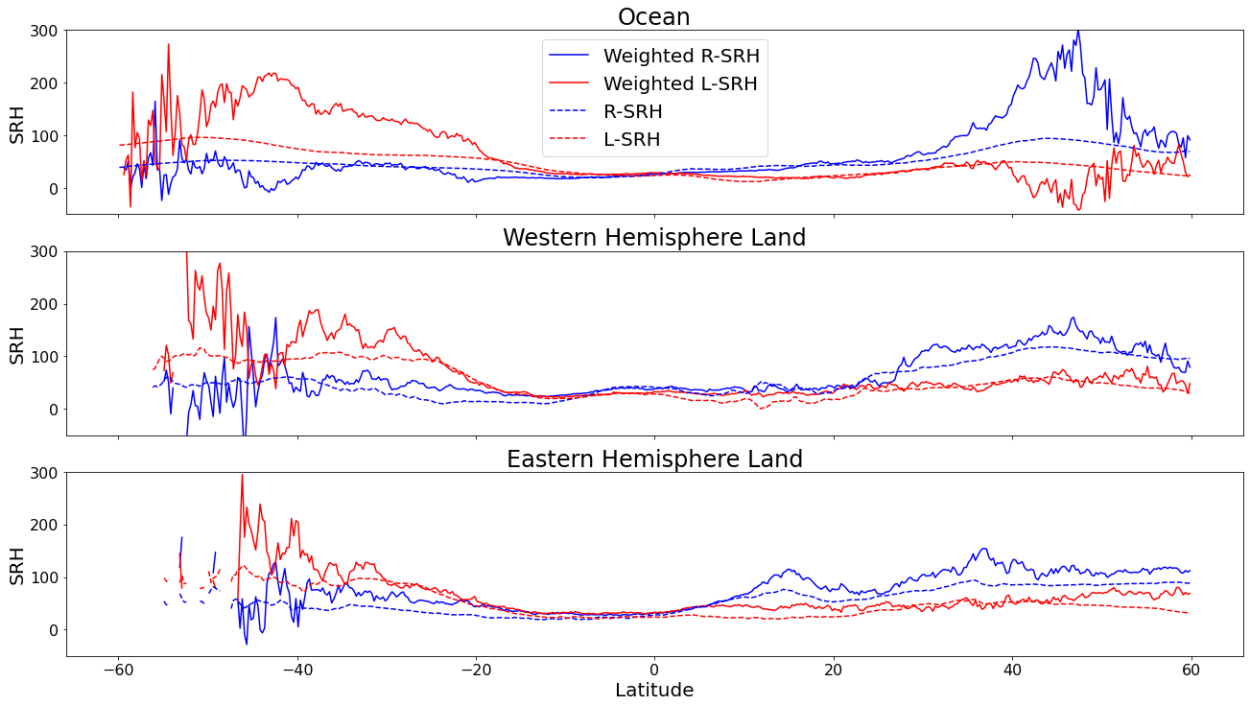

Figure 14. As in Figure 8 but for zonal-mean 0–3 km SRH (m^2 s^{-2}) for the right-moving (blue) and left-moving (red) storms. Solid lines are weighted by six-hourly $W_{up} > 10$ m s^{-1} counts in quarter-degree grid bins; dashed lines are the unweighted means. Negative L-SRH (favoring the left-mover) is plotted as positive values. The very large values of the weighted-mean SRH in the subpolar oceans come from a relatively small number of convective events.

Why does the ratio of cyclonic to anticyclonic storms increase with the threshold? We can speculate on the causes for this. It may be that stronger updrafts are able to tilt more of the (preferentially cyclonic) environmental shear into vertical vorticity, whereas weaker updrafts are more reliant on other processes (such as cold pool-generated vorticity) that will be more equitably of either sign. This would result in a significant number of anticyclonic weaker updrafts, which would have lower UH, but relatively few anticyclonic strong updrafts. Indeed this is typically what is seen over the CONUS: anticyclonic supercell storms tend to weaken more quickly under directional shear than does the cyclonic

supercell split from the same event. It may also be true that flow convergence may locally enhance the SRH to high levels, thereby inducing rotation within developing updrafts. This is akin to the result of Nolan (2011) who found VHTs whose strong rotation arose from local enhancement of SRH.

5 Conclusions

We have described the properties of rotating convection in the X-SHiELD global storm resolving model. The frequencies of intense convection (6-hour maximum updraft velocities of 10 m s^{-1} or greater) match the expected spatial and seasonal distributions, giving credence to the validity of our results. In all regions cyclonically rotating updrafts (counterclockwise in the northern hemisphere and clockwise in the southern) predominate over anticyclonic updrafts, a preference stronger over higher latitudes especially in the ocean. In the deep tropics there is a near equality in the counts of cyclonic and anticyclonic updrafts, with the ratio between cyclonic and anticyclonic increasing poleward until about 20 degrees latitude, leveling off at higher latitudes. This is complicated over the continents by the more complex geography, and several continental convective hot spots are present in which anticyclonic updrafts are common. Even over land cyclonic rotation is preferred nearly everywhere, a preference that only increases at higher UH thresholds.

An examination of marine convection over the western Pacific reveals that the rotating updrafts are individual thunderstorms embedded within convective clusters. Cyclonic storms predominate in the subtropics while there is near equality in the deep tropics, where many updrafts may not rotate at all. These individual thunderstorms are not sufficiently long-lived for planetary vorticity to directly affect storm formation, so we conclude that the synoptic-scale environment is likely the determining factor. There is a correspondence with the convection-weighted storm-relative helicity (SRH) of the appropriate sign and of the number of rotating storms in these clusters, indicating that some of the difference can be explained by synoptic conditions. X-SHiELD also produces numerous pairs of counter-rotating storms, indicating that baroclinic vorticity generation is taking place. We conclude that, similarly to the well-understood process leading to the origin of rotation in continental storms, the relative prevalence of cyclonic to anticyclonic storms arises from the ambient SRH in the synoptic environment for cyclonic storms (right-moving in the northern hemisphere) compared to that for anticyclonic storms. The synoptic systems in which the storms are embedded are long-lived enough to be affected by the planetary rotation, which will prefer one sign of environmental rotation at higher latitudes. This does not however rule out the appearance of either sense of updraft rotation for individual events. The analogy to mid-latitude continental convection should also not be taken too far as it is recognized that while some of the same processes may be at work (Hogsett and Stewart, 2014) the environments tend to be very different (Kilroy and Smith 2015).

This explanation does not consider the regional factors which complicate the pattern, especially over the mid-latitude continental hot spots in which the

preference for one sign of rotation is much less pronounced. Some of this variation can be explained by the climatological pattern of SRH, but there are areas especially in the continental sub-tropics where the preference for cyclonic updrafts is not associated with larger values of cyclonic SRH. One shortcoming of the current version of X-SHiELD is that convection may be over-intense, especially over the oceans where the model produces as much intense convection as is seen over the continents. Since intense convection is rarely seen over the ocean (Liu et al. 2007, Houze et al. 2015) this could point to some distinctive property of tropical convection the model is not yet picking up on, or possibly that observations are not sampling the most intense updrafts in oceanic convection. One challenge with GSRMs is that explicit convection cannot be "tuned" as is done with parameterized convection (Hourdin et al., 2017) and so producing convective statistics and upscale impacts to match those in the real atmosphere is more difficult. Another potential limitation of our results is that the evolution of baroclinically-generated counter-rotating pairs of storms is heavily dependent on specifics of cold pool structure (Grasso 2000), which in turn depends on the details of the microphysics and boundary layer schemes. This is illustrated by our results in the central plains of the United States, in which the model simulates a nearly equal number of cyclonic and anticyclonic updrafts for the weaker 50 m^2 s^{-2} threshold (Figure 3). This is despite the well-understood predominance of cyclonic rotation in severe convection, a distinction which is simulated by X-SHiELD (Figures 5, 7). Other mechanisms for creating local rotation, including convergence of vertical or horizontal vorticity (Nolan 2011) and the creation of shear zones, may also be at work. The potential model-dependence on updraft frequency, intensity, and rotation is a source of uncertainty in these results; Dauhut and Hohenegger (2022) came to a similar conclusion in their study of stratospheric hydration in a GSRM.

Future work could establish whether rotating updrafts have a broader significance in the earth system, including whether rotating updrafts are longer-lived worldwide. This could have significant implications for storm impacts and on the larger-scale impacts of intense convection. Regional seasonal variations in the two senses of UH (Northeastern Pacific, Gulf of Mexico, India) are of additional interest. The seasonal variation in severe weather events in the Southeastern US is well-studied and has a notable late-season secondary maximum in severe weather, and other areas may be of equal scientific and societal interest. GSRMs like X-SHiELD provide a new way to extend the traditional focus of rotating convection beyond severe continental convection and to give a broader view of the significance of this phenomenon, including how rotating convection may change in a warmer climate.

Acknowledgments

We thank JongIl Han at the Environmental Modeling Center (EMC) for providing and assisting with the latest version of the TKE-EDMF scheme, and George Gayno and Helin Wei also of EMC for assistance with high-resolution land model inputs. Daniel Klocke (Max Planck Institute for Meteorology) pro-

vided ECMWF analyzed SSTs. Ming Zhao and Stephen Garner (GFDL) provided insightful reviews materially improving this paper. Stephan Fueglistaler (Princeton University) encouraged this year-long simulation and both GFDL and CIMES management facilitated this project. Finally, we acknowledge S-J Lin's leadership in creating FV3 and the GSRM predecessors to X-SHiELD, and his generational talent and vision that led to the success of these models. Zhou and Cheng are supported under awards NA18OAR4320123, NA19OAR0220146, and NA19OAR0220147 from the National Oceanic and Atmospheric Administration (NOAA), U.S. Department of Commerce. Cheng's contributions are additionally supported by the Weather Program Office, Office of Oceanic and Atmospheric Research, NOAA. The statements, findings, conclusions, and recommendations are those of the authors and do not necessarily reflect the views of NOAA, or the U.S. Department of Commerce.

Open Research

Public releases of SHiELD are available at https://github.com/NOAA-GFDL/SHiELD_build. The code used for the version of X-SHiELD in this paper is given at https://doi.org/10.5281/zenodo.6941034. Data used to produce the figures is at https://doi.org/10.5281/zenodo.6949403. GPM data in Figure 6 are from Huffman et al. (2019). Tornado events in Figure 7b are from the Storm Events Database at https://www.ncdc.noaa.gov/stormevents.

References

Boucher, O., Servonnat, J., Albright, A. L., Aumont, O., Balkanski, Y., & Bastrikov, V., et al. (2020). Presentation and evaluation of the IPSL-CM6A-LR climate model. *Journal of Advances in Modeling Earth Systems*, 12, e2019MS002010. https://doi.org/10.1029/2019MS002010

Bunkers, M. J. (2002). Vertical Wind Shear Associated with Left-Moving Supercells. *Weather and Forecasting*, 17(4), 845-855.

Bunkers, M. J., Klimowski, B. A., Zeitler, J. W., Thompson, R. L., & Weisman, M. L. (2000). Predicting Supercell Motion Using a New Hodograph Technique. *Weather and Forecasting*, 15(1), 61-79.

Bunkers, M. J., Hjelmfelt, M. R., & Smith, P. L. (2006). An Observational Examination of Long-Lived Supercells. Part I: Characteristics, Evolution, and Demise. *Weather and Forecasting*, 21(5), 673-688.

Cheng, K.-Y., and coauthors (2022). Impact of warmer sea surface temperature on the global pattern of intense convection: insights from a global storm resolving model. *Geophysical Research Letters*, 49, e2022GL099796. https://doi.org/10.1029/2022GL099796

Dauhut, T., & Hohenegger, C. (2022). The contribution of convection to the stratospheric water vapor: The first budget using a global storm-resolving model. *Journal of Geophysical Research: Atmospheres*, 127, e2021JD036295. https://doi.org/10.1029/2021JD036295

Droegemeier, K. K., Lazarus S. M. , and Davies-Jones R. P. (1993). The influence of helicity on numerically simulated convective storms. *Monthly Weather Review*, **121 ,** 2005–2029.

Duras, J., Ziemen, F., & Klocke, D (2021). The DYAMOND Winter data collection. EGU21, https://doi.org/10.5194/egusphere-egu21-4687

Emanuel, K. A. (1989). Dynamical theories of tropical convection. *Australian Meteorological Magazine*, 37(1).

Gehne, M., Hamill, T. M., Kiladis, G. N., & Trenberth, K. E. (2016). Comparison of Global Precipitation Estimates across a Range of Temporal and Spatial Scales. *Journal of Climate,* 29(21), 7773-7795.

Grasso, L. D. (2000). The Dissipation of a Left-Moving Cell in a Severe Storm Environment. *Monthly Weather Review*, *128*(8), 2797-2815.

Grasso, L. D., & Hilgendorf, E. R. (2001). Observations of a Severe Left Moving Thunderstorm. *Weather and Forecasting*, *16*(4), 500-511.

Guimond, Stephen R., Gerald M. Heymsfield, and F. Joseph Turk (2010). Multiscale Observations of Hurricane Dennis (2005): The Effects of Hot Towers on Rapid Intensification. *Journal of the Atmospheric Sciences,* 67(3), 633-654. https://doi.org/10.1175/2009JAS3119.1 .

Han, Jongil, Marcin L. Witek, Joao Teixeira, Ruiyu Sun, Hua-Lu Pan, Jennifer K. Fletcher, and Christopher S. Bretherton (2016). Implementation in the NCEP GFS of a Hybrid Eddy-Diffusivity Mass-Flux (EDMF) Boundary Layer Parameterization with Dissipative Heating and Modified Stable Boundary Layer Mixing. *Weather and Forecasting,* 31(1), 341-352. https://doi.org/10.1175/WAF-D-15-0053.1.

Han, Jongil, and Christopher S. Bretherton (2019). "TKE-Based Moist Eddy-Diffusivity Mass-Flux (EDMF) Parameterization for Vertical Turbulent Mixing". *Weather and Forecasting* 34(4), 869-886. https://doi.org/10.1175/WAF-D-18-0146.1.

Harris, L., Zhou, L., Lin, S.-J., Chen, J.-H., Chen, X., Gao, K., et al. (2020). GFDL SHiELD: A unified system for weather-to-seasonal prediction. *Journal of Advances in Modeling Earth Systems*, 12, e2020MS002223. https://doi.org/10.1029/2020MS002223

Hendricks, E. A., Montgomery, M. T., & Davis, C. A. (2004). The Role of "Vortical" Hot Towers in the Formation of Tropical Cyclone Diana (1984). *Journal of the Atmospheric Sciences*, 61(11), 1209-1232.

Hitchens, N. M., Brooks, H. E., and Kay, M. P. (2013). Objective Limits on Forecasting Skill of Rare Events. *Weather and Forecasting* 28 (2), 525-534. https://doi.org/10.1175/WAF-D-12-00113.1

Hogsett, W. A., & Stewart, S. R. (2014). Dynamics of Tropical Cyclone Intensification: Deep Convective Cyclonic "Left Movers". *Journal of the Atmospheric Sciences*, 71(1), 226-242.

Hourdin, F., Mauritsen, T., Gettelman, A., Golaz, J., Balaji, V., Duan, Q., Folini, D., Ji, D., Klocke, D., Qian, Y., Rauser, F., Rio, C., Tomassini, L., Watanabe, M., & Williamson, D. (2017). The Art and Science of Climate Model Tuning. Bulletin of the American Meteorological Society, 98(3), 589-602.

Houze Jr., R. A., Rasmussen, K. L., Zuluaga, M. D., & Brodzik, S. R. (2015). The variable nature of convection in the tropics and subtropics: A legacy of 16 years of the Tropical Rainfall Measuring Mission satellite. Reviews of Geophysics, 53(3), 994–1021. https://doi.org/10.1002/2015RG000488

Huffman, G.J., E.F. Stocker, D.T. Bolvin, E.J. Nelkin, Jackson Tan (2019). GPM IMERG Final Precipitation L3 Half Hourly 0.1 degree x 0.1 degree V06. Greenbelt, MD, Goddard Earth Sciences Data and Information Services Center (GES DISC), Accessed: 4 August 2021, 10.5067/GPM/IMERG/3B-HH/06

Judt, F., D. Klocke, R. Rios-Berrios, B. Vanniere, F. Ziemen, L. Auger, J. Biercamp, C. Bretherton, X. Chen, P. Düben, C. Hohenegger, M. Khairoutdinov, C. Kodama, L. Kornblueh, S.-J. Lin, M. Nakano, P. Neumann, W. Putman, N. Röber, M. Roberts, M. Satoh, R. Shibuya, B. Stevens, P. L. Vidale, N. Wedi, and L. Zhou (2021). Tropical cyclones in global storm-resolving models. *Journal of the Meteorological Society of Japan*, 99, 579-602. https://doi.org/10.2151/jmsj.2021-029

Kain, J. S., Weiss, S. J., Bright, D. R., Baldwin, M. E., Levit, J. J., Carbin, G. W., Schwartz, C. S., Weisman, M. L., Droegemeier, K. K., Weber, D. B., & Thomas, K. W. (2008). Some Practical Considerations Regarding Horizontal Resolution in the First Generation of Operational Convection-Allowing NWP. *Weather and Forecasting*, *23*(5), 931-952.

Kilroy, G. Evolution of convective characteristics during tropical cyclogenesis (2021). *Quarterly Journal of the Royal Meteorological Soc*iety, 147, 2103– 2123. https://doi.org/10.1002/qj.4011

Kilroy, G. and Smith, R.K. (2015), Tropical cyclone convection: the effects of a vortex boundary-layer wind profile on deep convection. *Quarterly Journal of the Royal Meteorological Soc*iety, 141, 714-726. https://doi.org/10.1002/qj.2383

Liu, C., Zipser, E. J., & Nesbitt, S. W. (2007). Global Distribution of Tropical Deep Convection: Different Perspectives from TRMM Infrared and Radar Data. *Journal of Climate*, 20(3), 489–503. https://doi.org/10.1175/JCLI4023.1

Miyamoto, Y., Kajikawa, Y., Yoshida, R., Yamaura, T., Yashiro, H., and Tomita, H. (2013). Deep moist atmospheric convection in a subkilometer global simulation. *Geophysical Research Letters*, 40, 4922– 4926.

Nolan, D. S. (2011). Evaluating Environmental Favorableness for Tropical Cyclone Development with the Method of Point-Downscaling. *Journal of Advances in Modeling Earth Systems*, 3, M08001, doi:10.1029/2011MS000063

Nugent, J. M., Turbeville, S. M., Bretherton, C. S., Blossey, P. N. and Ackerman, T. P. (2022). Tropical cirrus in global storm-resolving models:

1. Role of deep convection. *Earth and Space Science*, 9, e2021EA001965. https://doi.org/10.1029/2021EA001965

Potvin, C. K., and coauthors (2019). Systematic Comparison of Convection-Allowing Models during the 2017 NOAA HWT Spring Forecasting Experiment. Weather and Forecasting, 34(5), 1395-1416.

Satoh, M., Stevens, B., Judt, F., Khairoutdinov, M., Lin, S.-J., Putman, W. M., & Düben, P. (2019). Global Cloud-Resolving models. *Current Climate Change Reports*, *5*(3), 172–184. https://doi.org/10.1007/s40641-019-00131-0

Tatsuya Seiki, Woosub Roh & Masaki Satoh (2022). Cloud Microphysics in Global Cloud Resolving Models. *Atmosphere-Ocean*, 60(3-4), 477-505.

Sobash, R. A., Kain, J. S., Bright, D. R., Dean, A. R., Coniglio, M. C., & Weiss, S. J. (2011). Probabilistic forecast guidance for severe thunderstorms based on the identification of extreme phenomena in convection-allowing model forecasts. *Weather and Forecasting*, 26(5), 714–728. https://doi.org/10.1175/WAF-D-10-05046.1

Stephan, C.C., Duras, J., Harris, L., Klocke, D., Putman, W.M., Taylor, M., Wedi, N.P., Žagar, N. and Ziemen, F., (2022). Atmospheric Energy Spectra in Global Kilometre-Scale Models. *Tellus A: Dynamic Meteorology and Oceanography*, 74, 280–299. http://doi.org/10.16993/tellusa.26.

Stevens, B., Satoh, M., Auger, L. et al. (2019). DYAMOND: the DYnamics of the Atmospheric general circulation Modeled On Non-hydrostatic Domains. *Progress in Earth and Planetary Science*, 6, 61. https://doi.org/10.1186/s40645-019-0304-z

Turbeville, S. M., Nugent, J. M., Ackerman, T. P., Bretherton, C. S. and Blossey, P. N. (2022): Tropical cirrus in global storm-resolving models: 2. Cirrus life cycle and top-of-atmosphere radiative fluxes. *Earth and Space Science*, 9, e2021EA001978. https://doi.org/10.1029/2021EA001978

Trapp, R. J., Stumpf, G. J., and Manross, K. L (2005). A Reassessment of the Percentage of Tornadic Mesocyclones. *Weather and Forecasting,* 20(4) (2005): 680-687. https://doi.org/10.1175/WAF864.1

Wang, Z. (2018). What is the Key Feature of Convection Leading up to Tropical Cyclone Formation? *Journal of the Atmospheric Sciences*, *75*(5), 1609-1629.

Wedi, N. P., Polichtchouk, I., Dueben, P., Anantharaj, V. G., Bauer, P., Boussetta, S., et al. (2020). A baseline for global weather and climate simulations at 1 km resolution. *Journal of Advances in Modeling Earth Systems*, 12, e2020MS002192. https://doi.org/10.1029/2020MS002192

Zawislak, J. (2020). Global Survey of Precipitation Properties Observed during Tropical Cyclogenesis and Their Differences Compared to Non-developing Disturbances. *Monthly Weather Review*, 148(4), 1585-1606. https://doi.org/10.1175/MWR-D-18-0407.1

Zhao, M., Golaz, J.-C., Held, I. M., Guo, H., Balaji, V., Benson, R., et al. (2018). The GFDL global atmosphere and land model AM4.0/LM4.0: 1. Simulation characteristics with prescribed SSTs. *Journal of Advances in Modeling Earth Systems*, 10, 691-734. https://doi.org/10.1002/2017MS001208

Zhou, L., S.-J. Lin, J.-H. Chen, L. M. Harris, X. Chen, and S. L. Rees (2019). Toward Convective-Scale Prediction within the Next Generation Global Prediction System. *Bulletin of the American Meteorological Society*,100, 1225-1243. https://doi.org/10.1175/BAMS-D-17-0246.1

Zhou, L., Harris, L., Chen, J.-H., Gao, K., Guo, H., Xiang, B., et al. (2022). Improving global weather prediction in GFDL SHiELD through an upgraded GFDL cloud microphysics scheme. *Journal of Advances in Modeling Earth Systems*, 14, e2021MS002971. https://doi.org/10.1029/2021MS002971